JBC Papers in Press. Published on August 13, 2020 as Manuscript RA120.013934
The latest version is at https://www.jbc.org/cgi/doi/10.1074/jbc.RA120.013934

Immunostimulation by *Lactobacillus kefiri* S-layer proteins with distinct glycosylation patterns requires different lectin partners

Mariano Malamud[1, 2†], Gustavo Cavallero[3, †], Adriana C. Casabuono[3], Bernd Lepenies[2], María de los Ángeles Serradell[1*], Alicia S. Couto[3,*]

From [1]Cátedra de Microbiología, Departamento de Ciencias Biológicas, Facultad de Ciencias Exactas, Universidad Nacional de La Plata (UNLP), 47 y 117, 1900, La Plata, Argentina; [2]University of Veterinary Medicine Hannover, Immunology Unit & Research Center for Emerging Infections and Zoonoses (RIZ), 30559 Hannover, Germany; [3]Universidad de Buenos Aires, Facultad de Ciencias Exactas y Naturales, Departamento de Química Orgánica - Consejo Nacional de Investigaciones Científicas y Técnicas (CONICET), Centro de Investigación en Hidratos de Carbono (CIHIDECAR), Intendente Güiraldes 2160, C1428GA, Ciudad Universitaria, Buenos Aires, Argentina.

Running title: *L. kefiri S-layer protein glycosylation on immune activation*

† Both authors contributed equally to this work
*To whom correspondence should be addressed:
María de los Ángeles Serradell
Email: maserr@biol.unlp.edu.ar
Alicia Susana Couto
E-mail: acouto@fcen.uba.ar

Keywords: *Lactobacillus kefiri;* S-layer protein; glycosylation

Abstract

S-layer (glyco)-proteins (SLPs) form a nanostructured envelope that covers the surface of different prokaryotes and show immunomodulatory activity. Previously, we have demonstrated that the S-layer glycoprotein from probiotic *Lactobacillus kefiri* CIDCA 8348 (SLP-8348) is recognized by Mincle (macrophage inducible C-type lectin receptor) and its adjuvanticity depends on the integrity of its glycans. However, the glycan´s structure has not been described so far. Herein, we analyze the glycosylation pattern of three SLPs, SLP-8348, SLP-8321, and SLP-5818, and explore how these patterns impacts their recognition by C-type lectin receptors (CLRs) and the immunomodulatory effect of the *L. kefiri* SLPs on antigen-presenting cells. HPAEC-PAD performed after β-elimination showed glucose as the major component in the *O*-glycans of the three SLPs, however, some differences in the length of hexose chains were observed. No N-glycosylation signals were detected in SLP-8348 and SLP-8321, but SLP-5818 was observed to have two sites carrying complex N-glycans based on a site-specific analysis and a glycomic workflow of the permethylated glycans. SLP-8348 was previously shown to enhance LPS-induced activation on both RAW264.7 macrophages and murine BMDCs; we now show SLP-8321 and SLP-5818 have a similar effect regardless of the differences in their glycosylation patterns. Studies performed with BMDCs from CLR-deficient mice revealed that the immunostimulatory activity of SLP-8321 depends on its recognition by Mincle, whereas SLP-5818's effects are dependent on SignR3 (murine ortholog of human DC-SIGN). These findings encourage further investigation of both the potential application of these SLPs as new adjuvants and the protein glycosylation mechanisms in these bacteria.

Introduction

Glycosylation is considered the most popular post-translational modification targeting proteins. Despite until the mid 70´s it was assumed that the ability to glycosylate proteins was restricted to

eukaryotic cells and archaebacteria (1), nowadays it is known that this post-translational modification is not an exception in eubacteria, although it is early to predict the full extent of prokaryotic glycosylation (2). From the studies performed on eukaryotic cells, it is clear that the presence of glycans affect expression, localization and lifetime of numerous proteins thus affecting its functions as well as several downstream biological events (3).

In eubacteria, protein glycosylation has been extensively studied in pathogens, emphasizing its relevance in virulence and pathogenicity. On the contrary, the nature and function of glycoproteins in non-pathogenic bacteria, including gut commensal species, remains largely unexplored (4). Since interactions between commensal bacteria, intestinal epithelial and immune cells play a crucial role in the maintenance of gut homeostasis, the study of protein glycosylation in gut commensal bacteria has become an expanding field of research due to the importance of the role of gut microbiota in health and disease (5, 6). This is particularly relevant in the case of surface proteins, which act as mediators of several interactions between microorganisms and their host.

The S-layer is a nanostructured proteinaceous envelope constituted by subunits that self-assemble to form a two-dimensional lattice that covers the surface of different species of *Bacteria* and *Archaea* (7). Given their ubiquitous presence, S-layers are considered as the result of evolutionary changes of the microorganisms to survive in harsh environments (8) although there are no reports on common functions for all of them (9). The presence of S-layer has been found in both Gram-negative and Gram-positive bacteria, including pathogenic and non-pathogenic species (10). Regarding the members of the genus *Lactobacillus*, microorganisms commonly retrieved in the gut of different mammalian hosts as well as in fermented foods, the S-layer has been detected in many but not all species (11). Due to their unique self-assembly ability, presenting repetitive identical physicochemical properties down to the subnanometer scale, the S-layer proteins have gain interest in distinct areas of biotechnology, biomimetic and biomedicine. Indeed, different researchers have been conducted experiments focusing on the application of S-layer proteins for the development of new antigen/hapten carriers, adjuvants or vaccination vesicles (11, 12).

After the presence of S-layer proteins in several strains of *L. kefiri* formerly isolated from kefir grains and characterized as potentially health-promoting microorganisms was described (13), several studies have been performed in our laboratory to gain knowledge about structural and functional properties of these surface proteins. In particular, the S-layer proteins from *L. kefiri* strains show differences in their amino acid sequences, mainly in the C-terminal region of the polypeptide (14). Moreover, they are part of the small group of glycosylated S-layer proteins reported within the genus *Lactobacillus* (11), and until now, the detailed glycan structures have been described just for the strain *L. kefiri* CIDCA 83111 (15).

Noteworthy, although the S-layer proteins were the first glycoproteins described in prokaryotes, the studies of the role of the glycan residues in the functional properties of these proteins are scarce and are usually focused on some archaea (16) or pathogenic bacteria (17,18). Regarding the genus *Lactobacillus*, there are some reports describing the involvement of the carbohydrate receptor DC-specific ICAM-3-grabbing nonintegrin (DC-SIGN) in the functional activity of the S-layer proteins from *L. acidophilus* NCFM (19), *L. plantarum* (20) and *L. kefiri* JCM 5818 (21). In this sense, we have recently demonstrated that the S-layer glycoprotein from *L. kefiri* CIDCA 8348 is able to enhance the LPS-induced response in murine macrophages in a carbohydrate-receptor mediated process (22). Moreover, this SLP improves the OVA-specific cell immune response by triggering maturation of antigen presenting cells through the recognition of glycan moieties by Mincle (23). However, the structure of its glycans has not been determined so far.

Considering all these evidences, in the present work we aim to determine the glycosylation patterns of the S-layer proteins expressed on different strains of *L. kefiri* and to analyze the impact on the immunomodulatory activity on antigen presenting cells.

Results

Glycan structures of *L. kefiri* S-layer proteins

We have previously reported the composition and structure of the glycans present in the S-layer protein from *L. kefiri* CIDCA 83111 (15). In this work, glycosylation of the S-layer protein from *L. kefiri* JCM 5818, CIDCA 8348 and CIDCA 8321 (SLP-5818, SLP-8348 and SLP-8321, respectively) were characterized. In this regard, the analysis of both *O*- and *N*-glycans was performed.

O-glycome analysis

The SDS-PAGE bands corresponding to the purified SLPs of each strain were subjected to reductive β-elimination. Sugar composition was achieved by HPAEC-PAD. For this purpose, the released oligosaccharides were hydrolyzed, and monosaccharides were determined. In the three SLPs examined glucose was detected as the major component (Figure 1A, B and C). Also, in the three cases, when an alditol analysis was performed, sorbitol was detected. Taking into account that during the treatment the oligosaccharides linking the peptide are released and the reducing end of the oligosaccharides are reduced by $NaBH_4$ to an alditol, the result indicates that a glucose unit is the linkage between the O-linked oligosaccharides and the peptides. (Figure 1D, E and F).

The O-glycoproteomic analysis of the SLPs was performed by nanoHPLC-ESI-Orbitrap-HCD. An *in-gel* trypsin digestion of the purified glycoprotein from each strain was performed followed by a glycopeptide enrichment step using cotton HILIC chromatography. In SLP-5818, the analysis of the extracted ion chromatogram showed a defined region of *O*-glycosylation detected by EICs of oxonium ions where up to four hexose units were detected (*m/z* =163.06; 325.11, 487.16, 649.21). It is known that glycosidic bonds are more labile under the HCD dissociation than peptides. However, notably in this case, a high coverage level of peptide fragmentation was achieved by detecting b and y ions from the glycosylated peptide. Moreover, peptide-glycan fragments (Y ions) and the ion corresponding to the naked peptide were also detected (Figure 2A). Deconvolution of the ions allowed the attribution of the signals eluting at retention time between 10-14 min to peptide ^{147}SASASSASSASSAEQTTALTDAQK^{170} carrying from 10 to 35 hexoses. Different glycoforms were resolved in the operating conditions of the RP nanoHPLC employed. It is clearly evidenced that the chromatographic elution of *O*-glycopeptides is based on the hydrophilic nature of the attached glycans, therefore on their decreasing size, from the largest to the smallest one. Interestingly, it was also possible to detect glycosylation from just one hexose unit co-eluting with the non-modified peptide (Figure 2B, Table 1), indicating that this *O*-glycosylation site is not fully occupied in this protein.

On the other hand, it was interesting to detect in EICs from both, SLP-8321 and SLP-8348 a region where several clusters of ions with charge +4, +5, +6 and +7 corresponding to peptide 125-170 containing the SASSASASA motif bearing up to 26 hexose units (Figure 3A, B, Tables 2 and 3). MS/MS spectrum of the different ions showed b- and y- peptide fragments, confirming the peptide identification (Figure 3C, D).

L. kefiri JCM 5818 N-glycome analysis

Further on, taking into account that the S-layer protein of *L. kefiri* 83111 presented N-glycosylation (15) we searched for diagnostic oxonium ions for $HexNAc^+$ (*m/z* 204.09, *m/z* 168.07 and *m/z* 138.05) in the MS/MS spectra. No signals were detected for SLP-8348 and SLP-8321, however SLP-5818 evidenced the presence of the reporter ions.
Therefore, we first tried an affinity-based purification of the SLP of *L. kefiri* JCM 5818 using immobilized Wheat Germ Agglutinin (WGA) to evidence this type of posttranslational modification. Interestingly, although whole protein fraction showed that the purification was not complete (Figure 4A, lane 2), the SDS-PAGE profile from the lectin-bound fraction showed a protein band with MW 67 kDa in accordance with the reported MW of the SLP-5818 (24,25) (Figure 4A, lane 1). This band was excised, trypsin-digested and subjected to mass spectrometry analysis confirming the S-layer protein identity and thus, the presence of N-glycosylation in this protein (Supplemental 1 shows protein identification data).

In order to determine the *N*-glycosylation sites in SLP-5818, we used PNGase F to release the *N*-

glycans. It is known that the glycosylated asparagine residue is converted to aspartic acid during the enzymatic reaction (26). As a result, a mass increase of 0.984 Da is obtained in the modified peptide. Based on this strategy, a sample of enriched glycopeptides from SLP-5818 was *N*-deglycosylated using PNGase F and analyzed by nanoHPLC-ESI-Orbitrap. Due to the fact that spontaneous deamidation might occur, the ratio asparagine/aspartic acid was considered in order to avoid misassignments (Supplemental 2 shows peptide identification data). Thus, two *N*-glycosylation sites at NVAV**N**^{55}GTNALYTK and at DAALTSL**N**^{457}NTVK were determined. As shown in Figure 4B, MS2 spectrum of peptide NVAV**N**^{55}GTNALYTK showed fragment ion y_9 with a *m/z* = 982.48 (calc. *m/z* = 981.50, Δ 0.984 Da) confirming the *N*-glycosylation site at N^{55}. In the same way, MS2 spectrum of peptide DAALTSL**N**^{457}NTVK showed y_5- fragment ion *m/z* = 576.30 (calc. *m/z* = 575.31, Δ 0.984 Da) evidencing an *N*-glycosidic linkage in N^{457} (Figure 4C). Further on, in order to determine the *N*-glycan structures attached to SLP-5818, we performed an enzymatic hydrolysis of the *N*-oligosaccharides using PNGase F. Glycans were separated, permethylated and analyzed by nanoHPLC-ESI-Orbitrap. The extracted ion chromatograms corresponding to *m/z* = 464.24 (HexNAc-Hex$^+$), and *m/z* = 189.11 (dHex$^+$) allowed to detect a family of complex permethylated *N*-glycans eluting between Rt 40-45 min (Figure 5A). Main structures, *m/z* and mass errors are detailed in Table 4. Figure 6 shows two examples of MS2 spectra of selected ions assigned to two bi-antennary glycans differing in the composition of one antennae. The permethylated *N*-glycans were also examined using MALDI-TOF MS and structures corresponding to bi-antennary species were also detected (Figure 5B).

Stimulation of murine macrophages by *L kefiri* SLPs

Regarding that we have previously demonstrated that SLP-8348 can enhance LPS-induced activation of antigen presenting cells (22,23), we decided to test the ability of SLP-8321 and SLP-5818 to activate murine macrophage, using RAW 264.7 cells as first model. As it was previously observed for SLP-8348 (22,23), the SLP-8321 and SLP-5818 were not able to induce activation of RAW 264.7 cells by themselves. However, respective significant increments in secreted IL-6 as well as in surface expression of CD40 and CD86 were observed for macrophages simultaneously exposed to *E. coli* LPS and *L. kefiri* S-layer glycoproteins in comparison to LPS-treated cells (Figure 7A, B). To note, no significant differences were observed among the stimulatory activity of strains despite the differences in their glycosylation patterns.

Interaction of SLPs with different C-type lectin receptors

Considering that it has been previously shown for SLP-8348 that the recognition of the glycan residues by a C-type lectin receptor (CLR) is a key event in the immunomodulatory activity of the protein (23), we decided to test the ability of SLP-8321 and SLP-5818 to interact with different CLRs. As shown previously for SLP-8348 (23), SLP-8321 and SLP-5818 bound to the CLRs DC-SIGN, SingR3, Langerin and Mincle (Figure 8A). As expected, a reduction of approximately 70% was observed in the SLP-CLR interactions in the presence of the Ca^{+2} chelating agent EGTA (Figure 8B).

Activation of BMDC by SLP-8321 and SLP-5818

Regarding the ability of SLP-8321 and SLP-5818 to interact with different CLRs and considering that both glycoproteins enhanced LPS-induced response in murine macrophages, we decided to use BMDC from C57BL/6 mice as antigen presenting cells to assess both internalization of SLPs and cell activation. As shown for SLP-8348 (23), we observed that both SLP-8321 and SLP-5818 were internalized by BMDC in a dose-dependent way (Figure 9A). However, a significant decrease in the uptake of SLP-8321 was observed when BMDC from Mincle$^{-/-}$ mice were used. On the contrary, the internalization of SLP-5818 was only reduced in BMDC from SignR3$^{-/-}$ mice and was not affected by the absence of Mincle (Figure 9A).

Following the same methodology previously reported (23), we decided to test the immunomodulatory activity of SLP-8321 and SLP-5818 on BMDCs. Unlike in the case of RAW 264.7

cells, both SLPs were able to induce the maturation of BMDC since a significant increment in the level of secreted IL-6 and TNF-α as well as in the surface expression of CD40 and CD80 were observed (Figure 9B, C). The same effect was observed when BMDC were stimulated by a combination of SLPs and LPS. The stimulatory activity of SLP-8321 was lost when BMDC from Mincle$^{-/-}$ mice were used, whereas SLP-5818 was not able activate BMDC from SignR3$^{-/-}$ mice (Figure 9B, C).

To further investigate the T-cell stimulatory function of the SLP-activated BMDCs, OVA-treated BMDCs from wild type, Mincle$^{-/-}$, SignR3$^{-/-}$ and CARD9$^{-/-}$ were incubated in the presence or absence of SLP-8321 or SLP-5818 with purified T cells from OT-II mice, as was previously performed with SLP-8348 (23). Both SLPs could enhance the OVA-specific T cell response since a higher IFN-γ secretion as well as higher CD4^{+}T cell proliferation were observed upon simultaneous stimulation of wild type BMDCs with OVA and SLP-8321 or SLP-5818 compared to OVA-treated antigen presenting cells (Figure 10A,B). The absence of Mincle abrogated the immunostimulatory activity of SLP-8321 while SLP-5818 was not able to enhance CD4^{+}T cell response when BMDCs from SignR3$^{-/-}$ mice were used (Figure 10A,B). As was expected, none of the SLPs assessed were able to potentiate CD4^{+}T cell activation when assays were performed using BMDC from CARD9$^{-/-}$ mice, a downstream signaling protein of Mincle and SignR3 (27) (Figure 10A, B).

Discussion

Considering the ubiquitous presence of S-layer-carrying microorganisms and the abundance of the S-layer proteins, it is evident that these structures reflect the evolutionary adaptation of the organisms to natural habitats and must have provided them with advantages in specific environmental and ecological conditions (8). Glycosylation is the post-translational modification most frequently found in SLPs, a feature shared with other surface exposed proteins such as flagellin and pilin. Within the genus *Lactobacillus*, the glycoprotein nature of the S-layer proteins has been reported for strains of *L. buchneri* (28, 29), *L. plantarum* 41021/252 (28) *L. acidophilus* NCFM (19), *L. acidophilus* ATCC 4356 (30), and several strains of *L. kefiri* (14,24). In this last species, we have previously described the composition and structure of the O- and N-glycans present in the SLP of the strain *L. kefiri* CIDCA 83111 (15). Herein, we show that SLP-5818 also presents *O*- and *N*-glycosylated chains. In this case, peptide 147-170 is *O*-glycosylated in average with eight hexose units, but at difference with the SLP from *L. kefiri* CIDCA 83111, is not decorated with galacturonic acid (15). Regarding *N*-glycans, both SLP 5818 and SLP 83111 present two N-glycosylation carrying bianntenary chains.
On the other hand, SLP-8321 and SLP-8348 show 100% of homology at primary sequence level (14) and despite they present six potential N-glycosylation sites, no evidence of bearing N-glycans was found. On the contrary, *O*-glycosidic chains constituted by 4 to 12 glucose units were detected in both SLPs.

Inter-strain differences in the glycosylation patterns of SLP were also seen some years ago in *Thermoanaerobacter thermohydrosulfuricus* and *Thermoanaerobacterium thermosaccharolyticum* (31). Moreover, in *Clostridium difficile* the presence of a glycosylated SLP was only demonstrated in the strain Ox247 which encodes a putative glycosylation locus (18), while normally most *C. difficile* strains do not possess a glycosylated S-layer (32). On the other hand, Anzengruber and coworkers reported that SlpB from *L. buchneri* CD034, SlpN from *L. buchneri* NRRL B-30929 and *L. buchneri* SlpB from 41021/251 showed identical *O*-glycans consisting of on average seven glucoses at four serine residues within the sequence S_{152}-A-S_{154}-S_{155}-A-S_{157} without any evidence of the presence of *N*-glycosidic chains in those SLP (29). In this sense, SLP-8321 and SLP-8348 show a higher similarity to the SLPs from *L. buchneri* strains than SLP-83111 and SLP-5818. Further studies are needed in order to elucidate the mechanisms through which the glycan chains are coupled to the peptide backbone in these surface proteins.

As surface exposed structures, the SLPs could be a key mediator between bacteria and host immune system contributing to the shaping of the immunological response to pathogenic, commensal and probiotic microorganisms. By using murine macrophages RAW 264.7 cells as model, we have demonstrated that despite the differences between

glycosylation patterns of SLP-8321 and SLP-5818, both proteins are able to enhance LPS-induced cell activation (Figure 7), similarly to previously demonstrated for SLP-8348 (22). These results suggest that *O*-glycans present in these three mentioned *L. kefiri* SLPs could be responsible, at least in part, of their immunostimulatory ability.

On the other hand, as previously described with SLP-8348 (23), the assays using BMDCs from Mincle$^{-/-}$ and SignR3$^{-/-}$ mice allowed us to determine that the internalization of SLP-8321 and SLP-5818 as well as their ability to activate BMDCs were mainly mediated by Mincle and SignR3 (the murine ortholog of human DC-SIGN), respectively (Figure 9), which could be expected considering the differences in the glycosidic moieties present in those proteins. Moreover, the incubation of BMDCs with SLPs from different *L. kefiri* strains leading to the enhancement of activation of OVA-specific CD4+T cells from OT-II mice, is also dependent of the presence of Mincle and SignR3 for SLP-8321 and SLP-5818, respectively (Figure 10). Some years ago, a pioneering work performed using a SlpA-knockout mutant *L. acidophilus* NFCM revealed that recognition of SlpA by DC-SIGN in presence of LPS induce an anti-inflammatory response in human monocyte-derived dendritic cells (19) suggesting the involvement of glycans in the immunomodulatory properties of SLPs. More recently, it was demonstrated that *L. acidophilus* NCK2187, a strain which solely expresses SlpA, and its purified SlpA binds to SignR3 to trigger regulatory signals that result in mitigation of experimental colitis, maintenance of healthy gastrointestinal microbiota, and mice protection (33). In addition, the ability of DC-SIGN to recognize the SLP-5818 was recently suggested by Prado Acosta and colleagues (21), which agrees with our findings. However, the role of glycan residues as well as the CLR involved in the internalization and immunostimulatory activity of the SLP-5818 had not been reported so far. On the contrary, is not surprising that Mincle, the CLR responsible for the recognition and adjuvanticity of the SLP-8348 (23), mediate the immunostimulatory effect of SLP-8321 on BMDCs since both glycoproteins present not only the same amino acid sequence (14) but also the same O-glycans. It is known that Mincle recognizes diverse sugar-containing ligands including trehalose dimycolate glycolipid from mycobacteria, mannose-, glucose- or fucose-containing glycoconjugates, and Lewis antigen from *Helicobacter pylori* LPS (34). To note, it was recently reported that Mincle also recognize the O-linked oligosaccharides of the SLP from the Gram-negative oral pathogen *Tannerella forsythia*, and that interaction induces both pro- and anti-inflammatory cytokine secretion in macrophages (17).

To resume, despite the differences in glycosylation patterns as well as the involvement of different CLRs, the glycosylated SLPs from distinct *L. kefiri* strains can induce activation of antigen presenting cells through the recognition of their glycans. Taken together, these findings encourage us to further investigate the potential application of these surface proteins derived from probiotic bacteria to the development of new adjuvants or carrier for vaccine antigens as well as to get deeper insight the protein glycosylation mechanisms in these bacteria.

Experimental procedures

Bacterial strains and culture conditions

Lactobacillus kefiri CIDCA 8321, and 8348 belonging to the collection of the Centro de Investigación y Desarrollo en Criotecnología de Alimentos (CIDCA) (35), and *L. kefiri* JCM 5818 were used. Bacteria were cultured in deMan-Rogosa-Sharpe (MRS)-broth (DIFCO, Detroit, USA) at 37°C for 48h, under aerobic conditions.

S-layer protein extraction

Extraction from bacterial cells at stationary phase was performed using 5M lithium chloride (LiCl) as described previously (22). The samples were centrifuged and the protein concentration in the supernatant was determined according to Bradford. The homogeneity of the protein extracts was tested by SDS-PAGE, stained with Coomassie blue (36). S-layer proteins were filtrated through a membrane of 0.22 µm pore diameter for cellular stimulation assays.

Composition and structure of glycan moieties

Lectin-based N-glycoprotein purification. The enrichment of glycoproteins was performed using Wheat Germ Agglutinin (WGA) lectin affinity chromatography. Briefly, 1 mL of WGA - Sepharose (Sigma) was loaded onto a 5 mL column. Prior to sample purification, stationary phase was equilibrated with 20mM Tris pH 7.5, 0.5M NaCl, 1mM $CaCl_2$, 1mM $MgCl_2$. Then, 50 µL of protein sample was loaded using the latter buffer solution. Non-glycosylated proteins were washed using 20mM Tris pH 7.5 containing 1M NaCl, 1mM $CaCl_2$, 1mM $MgCl_2$. Finally, the retained glycoproteins were eluted using the above buffer solution containing 0.5M *N*-Acetyl-D-Glucosamine. The glycoprotein fraction was dialyzed against ultra-pure water using Spectra/Por® (Repligen) molecular porous membrane tubing cut-off 3.5 kDa. The lectin-based purification was monitored by SDS-PAGE and stained with Colloidal Coomassie Blue.

Release of N-glycosidic chains by PNGase F treatment. The SDS-PAGE S-layer glycoprotein band was cut out from the gel, frozen for 3 h, and successively washed with (a) acetonitrile, (b) 20 mM $NaHCO_3$, pH 7, and (c) acetonitrile. The gel pieces were dried and the *N*-glycans were released by incubation with PNGase F (20 milliunits) (New England Biolabs Inc., Beverly, MA) overnight at 37 °C in 20 mM $NaHCO_3$, pH 7. The gel pieces were thoroughly washed, the supernatants were separated and filtered through an Ultrafree McFilter (Mr 5000), dried, resuspended in 0.1% (v/v) formic acid (20 µL), and left at room temperature for 40 min. Finally, glycans were dried and suspended in water.

Glycoprotein digestion. The protein band corresponding to the S-layer glycoproteins were cut out from the gel and washed with acetonitrile. The gel pieces were reduced with 10 mM DTT in 50 mM NH_4HCO_3 at 55 °C for 30 min. They were further washed with acetonitrile and alkylated with 55 mM IAA in 50 mM NH_4HCO_3 for 20 min at room temperature in darkness. After washing the gel pieces with 50 mM NH_4HCO_3 for 10 min and with acetonitrile for 5min, they were dried in a SpeedVac and submitted to digestion with 20 ng/µL trypsin (Sigma) in 40 mM NH_4HCO_3, 9 % acetonitrile at 37 °C overnight. Afterwards, the supernatants were separated and dried.

In gel-reductive β-elimination and sugar analysis. *O*-linked glycans were released from each SDS-PAGE band of the S-layer glycoproteins using 0.05M NaOH / 1M $NaBH_4$ and incubated overnight at 50°C. The solution was separated, acetic acid was added until pH 7 followed by repeated evaporation with methanol. The sample was dissolved in water, desalted in a Dowex 50 W (H^+) (Fluka) column and dried in SpeedVac. The β-eliminated samples were further hydrolyzed in 2 N TFA for 4 h at 100 °C. The acid was eliminated by evaporation and the hydrolysates were re-suspended in water for HPAEC-PAD (high performance anion exchange chromatography). Analysis was performed using a DX-500 Dionex BioLC system (Dionex Corp.). For neutral and amino sugars, a CarboPac PA20 with the corresponding guard column was used. Isocratic separations were achieved with 18mM NaOH and flow rate set to 0.4 mL/min. For alditols, a CarboPac MA 1 column was used with a 0.4 M NaOH isocratic program and a flow rate of 0.4 mL/min.

Permethylation of released oligosaccharides. After PNGase digestion, the oligosaccharides were methylated with NaOH in DMSO followed by addition of CH_3I as described (37).

Glycopeptide enrichment. Sample purification and glycopeptide enrichment was achieved by solid-phase extraction Cotton-HILIC microtips as described (38). Briefly, HILIC microtips were equilibrated with three volumes of 85% ACN. Dried sample was resuspended in 85% acetonitrile. Prior to SPE clean-up step, sample was loaded onto the stationary phase by aspirating and dispensing the protein mixture. Peptides were washed off from the column with 85% ACN, 0.5% TFA, and the retained glycopeptides were eluted using water. The glycopeptide fraction was freeze-dried and stored at -20°C until mass spectrometry analysis.

Mass spectrometry analysis. The enriched glycopeptide mixtures were re-suspended in 50% acetonitrile -1% formic acid/water 1:1. The digests were analyzed in a nanoLC 1000 coupled to an EASY-Spray Q Exactive Mass Spectrometer (Thermo Scientific) with a HCD (High Collision Dissociation) and an Orbitrap analyzer. An Easy Spray PepMap RSLC C18 column (50 µm × 150 mm, particle size 2.0 µm, pore size: 100 Å) at 40 °C

was used. Separation was achieved with a linear gradient from 5% to 35% solvent B developed in 75 min, at a flow of 300 nL/min (mobile phase A: water-0.1% formic acid; mobile phase B: acetonitrile-0.1% formic acid). Injection volume 2 µL. Spray voltage (+): 3.5 kV; (−): 3.0 kV. A full-scan survey MS experiment (*m/z* range from 400 to 2000; automatic gain control target 3 106; maximum IT: 200 ms, resolution at 400 *m/z*: 70000. Data Dependent MS2 method was set to the centroid mode, resolution 17500; maximum IT 50ms; automatic gain control target 105; fragment the top 15 peaks in each cycle; NCE: 27.
For the analysis of permethylated oligosaccharides HPLC separation was achieved with a linear gradient of solvent B from 5% to 60% developed in 75 min, flow: 300 nL/min (solvent A: water-0.1% formic acid; solvent B: ACN-0.1% formic acid). Injection volume: 5 µL.

MALDI-TOF MS (matrix-assisted laser desorption/ionization time-of-flight mass spectrometry analysis). Measurements were performed using an Ultraflex II TOF/TOF mass spectrometer (Bruker Daltonics GmbH, Bremen, Germany) equipped with a solid-state laser (λ = 355 nm). The system was operated by the Flexcontrol 3.3 package (Bruker Daltonics GmbsH, Bremen, Germany) using gentisic acid as matrix.

Data Analysis. Proteome Discoverer 2.1 (Thermo Scientific) assisted protein identification. The mass tolerances for MS and MS/MS were 10 ppm and 0.02 Da respectively. Missed cleavages allowed for tryptic digestion was 1. Carbamidomethylation of cysteine residues was set as static modification and oxidation of methionine as dynamic modification. For *N*-glycosite analysis conversion of asparagine to aspartic acid was included as dynamic modification. Precursor mass tolerance was 10 ppm, and fragment mass tolerance was 20 ppm. Confident identification for peptides was set to a score > 100.
Glycopeptide search was performed with MaxQuant version 1.6.5, Byonic™ from ProteinMetrics, Proteome Discoverer 2.2 and using a semi-automatic home-made software. (A0A1C3S3I4 S-layer protein OS=Lactobacillus kefiri OX=33962 GN=S-layer A0A1C3S3T6 S-layer protein OS=Lactobacillus kefiri OX=33962 GN=S-layer.
All glycopeptides identifications from both searches were manually curated. MS-Convert Tool (from ProteoWizard platform tools) converted raw data from enriched glycopeptides into text files for manual annotation. Deconvolution was assisted by Xtract on Thermo Xcalibur 3.0.63.

C-type Lectin Receptor recognition of S-layer proteins

The CLR-reactivity on S-layer proteins from *L. kefiri* CIDCA 8321 (SLP-8321) and *L. kefiri* JCM 5818 (SLP-5818) was evaluated by an ELISA type assay as described previously (23,39). A half-area microplate (Greiner Bio-One GmbH, Frickenhausen, Germany) was coated with 0.25 µg of SLP per well for 16 h at 4ºC and blocked with 1%BSA (Thermo Fisher Scientific, Darmstadt, Germany) for 2 h at room temperature (RT). Then, 0.25 µg of each CLR-hFc fusion protein in lectin-binding buffer (50 mM HEPES, 5 mM $MgCl_2$, and 5 mM $CaCl_2$) was added and incubated for 1 h at RT. For inhibition assays, CLR-hFc fusion proteins were pre-incubated with 5mM of EGTA (Sigma-Aldrich, USA). After washes, HRP-conjugated anti-human IgG anti-body (Dianova) was added to each well for 1 h at RT. Finally, plates were incubated with chromogenic substrate (o-phenylenediamine dihydrochloride substrate tablet (Thermo Fisher Scientific), 24 mM citrate buffer, 0.04% H_2O_2, 50 mM phosphate buffer in H_2O). The reaction was stopped with 2.0 M sulfuric acid and the product was read at 495 nm using a Multiskan Go microplate spectrophotometer (Thermo Fisher Scientific).

Mice

The source of the CLR- and CARD9-deficient mice was described previously (40,41,42). Mincle$^{-/-}$, SignR3$^{-/-}$ and CARD9$^{-/-}$ mice were backcrossed on C57BL/6 background over ten generations in the animal facility of the Federal Institute for Risk Assessment (Berlin, Germany). All mouse lines (including wild-type and C57BL/6-Tg (TcraTcrb)425Cbn/J (OT-II) mice) were kept in the animal house of the University of Veterinary Medicine (Hannover, Germany) with water and food supplied ad libitum. Mice were sacrificed for the isolation of spleen cells (OT-II transgenic mice)

or the preparation of bone marrow for BMDC generation (Mincle$^{-/-}$, CARD9$^{-/-}$, SignR3$^{-/-}$, and WT mice). Sacrificing of mice for scientific purposes was approved by the Animal Welfare Officers of the University of Veterinary Medicine Hannover (AZ 02.05.2016).

Cell cultures

The monocyte/macrophage murine cell line RAW 264.7 was cultured in Dulbecco's Modified Eagle Medium (DMEM) supplemented with: 10% (v/v) heat-inactivated (30 min/60◦C) fetal bovine serum(FBS), 1% (v/v) non-essential amino acids and 1% (v/v) penicillin-streptomycin solution (100 U/mL penicillin G, 100 g/mL streptomycin). All cell culture reagents were from GIBCO BRL Life Technologies (Rockville, MD, USA).
Bone marrow-derived dendritic cells (BMDCs) were generated from C57BL/6 wild type, Mincle $^{-/-}$, CARD9$^{-/-}$ or SignR3 $^{-/-}$ bone marrow precursors (2.5×10^5 cells/ml) that were plated in complete culture medium (IMDM supplemented with 2mM glutamine, 10% (v/v) FBS, 100 U/ml penicillin and 100µg/ml streptomycin) supplemented with a GM-CSF containing supernatant fromP3-X63 cells. Medium was exchanged every 48 h and BMDCs were used after 8–10 days of differentiation to ascertain that ≥80% of the cell population expressed the marker CD11c (43).

Cells stimulation assays

These experiments were performed as previously described (22,23). RAW 264.7 cells (2.5×10^5) were distributed onto 24-well microplates (JET BIOFIL®, China), and the medium volume was adjusted to 0.5mL. The plates were incubated for 48 h at 37◦C in a 5% CO2 95% air atmosphere to allow cell adherence prior to experimentation. After that, cells were treated with SLP-8321 or SLP-5818 (10µg/mL), in the presence or absence of LPS 0.1µg/mL (LPS from *Escherichia coli* O111:B4, SIGMA, USA), in DMEM for 24 h at 37ºC in a 5% CO_2 95% air atmosphere. Cells were incubated with anti-CD40 (3/23), anti-CD86 (P03.1) and then analyzed by flow cytometry.
BMDCs from wild type or CLR-deficient mice (1×10^5 cells/well) were distributed onto 96-well microplates (Sarstedt, Germany) and stimulated with SLP-8321 or SLP-5818 (10µg/mL), LPS (0.25µg/mL) or the combination of both for 16 h at 37ºC in a 5%CO_2 95%air atmosphere. Culture supernatants were collected and analyzed by ELISA for IL-6 and TNF-α secretion. Cells were incubated with anti-CD16/32 (93) to block cell surface FcgRII/RIII receptors, stained with anti-CD11c (N418), CD40 (3/23), CD80 (16-10A1) and then analyzed by flow cytometry.

BMDCs/T cell co-culture assay

Splenocytes were isolated from OT-II transgenic mice by flushing the spleen with complete IMDM medium. After erythrocyte lysis, cells were resuspended in MACS buffer (0.5% BSA, 2 mM EDTA in PBS). T cells were obtained by magnetic-activated cell separation (MACS) using Pan T cell isolation kit II, mouse (Miltenyi Biotech, Bergisch Gladbach, Germany) according to the manufacturer's instructions. T cells were labelled with CFSE (carboxyfluorescein diacetate succinimidyl ester, Sigma-Aldrich,USA) and seeded on a 96-well round bottom culture plate ($7x10^4$ cells/well). After 30 minutes, BMDCs treated with OVA (Endo Grade® Ovalbumin, LIONEX GmbH, Germany) or OVA/SLPs were added and incubated for 72 h. Culture supernatants were collected for IFN-γ secretion. Proliferation index of $CD4^+$ T cells within each experimental group was calculated as the ratio between the percentage of $CFSE^{low}$ $CD4^+$ cells and $CFSE^{low}$ $CD4^+$ cells from OVA-treated BMDCs.

Cytokine quantification in culture supernatants

Production of IL-6 by macrophages was analyzed by ELISA from BD-Pharmingen (San Diego, USA). Secretion of IL-6 and TNF-α by BMDCs and IFN-γ from purified T cells were analyzed by ELISA from PeproTech (USA). The assays were performed according to the manufacturer's instructions. After determining optical densities, cytokine levels in cell culture supernatants were calculated using the GraphPad Prism 7.0 program.

Immunocytostaining and flow cytometry

After stimulation experiments, cells were washed twice with PBS containing 2% (v/v) FBS and then labelled with specific monoclonal antibodies for 30min at 4◦C. Cells were washed twice and then

fixed with 1% (v/v) formaldehyde. Cells were analyzed using a FACSCalibur Analyzer (BD Biosciences) or Attune NxT Flow Cytometer (Thermo Fisher Scientific). Data analysis was performed using the FlowJo Software (FlowJo, Ashland, OR, USA).

Statistical analysis

Values from at least three independent experiments were analyzed by using a one-way or two-way ANOVA with Tukey's post hoc test ($P<0.05$ was considered statistically significant). Statistical analysis was performed with the GraphPad Prism program (GraphPad Software, San Diego, California, USA).

Data availability: The mass spectrometry proteomics data have been deposited to the ProteomeXchange Consortium via the PRIDE [44] partner repository with the dataset identifier PXD020358.

Authors contribution

MM performed the immunomodulatory assays, analyzed data, contribute with manuscript´s writing and revised the manuscript; GC performed the structural analysis, wrote the manuscript and revised it; AC contributed with the structural determination; BL conceived and supervised immunomodulatory assays, and revised the manuscript; MAS conceived the work, supervised immunomodulatory assays, and wrote the manuscript; and ASC conceived the work, supervised the structural analysis, and wrote the manuscript.

Funding and additional information

This work was supported by the Consejo Nacional de Investigaciones Científicas y Técnicas Grant PIP-11220110100660 (to GC, AC, ASC), Agencia Nacional de Promoción Científica y Tecnológica (ANPCyT) Grants PICT 2013-0736 (to GC, AC, ASC) and PICT 2016-0244 (to MM, MAS), Universidad de Buenos Aires Grant 20020130100476BA (to GC, AC, ASC), and Universidad Nacional Arturo Jauretche Grant 80020170100031UJ (to MM, MAS). The Ultraflex II (Bruker) TOF/TOF mass spectrometer was supported by ANPCyT Grant PME 125 (to GC, AC, ASC) and the ESI-Orbitrap by ANPCyT Grant PME 2012(CEQUIBIEM) (to GC, AC, ASC). Gustavo J. Cavallero and Mariano Malamud are fellows from ANPCyT and CONICET respectively. Alicia S. Couto and María de los Ángeles Serradell are members of Carrera de Investigador Científico y Tecnológico of CONICET. Mariano Malamud was also supported by funding from the German Academic Exchange Service (DAAD).

Conflict of Interest: The authors declare no conflicts of interest concerning this manuscript.

References

1. Messner, P., and U.B. Sleytr. (1992) Crystalline bacterial cell-surface layers. *Adv Microb Physiol* **33,** 213-275
2. Dell, A., Galadari, A., Sastre, F., and Hitchen, P. (2010) Similarities and differences in the glycosylation mechanisms in prokaryotes and eukaryotes. *Int J Microbiol* **2010**, 148178
3. Schäffer, C., and Messner, P. (2017) Emerging facets of prokaryotic glycosylation. *FEMS Microbiol Rev* **41**, 49-91
4. Latousakis, D., and Juge, N. (2018) How sweet are our gut beneficial bacteria? A focus on protein glycosylation in *Lactobacillus. Int J Mol Sci* **19**, 136
5. Lavelle, A., and Hill, C. (2019) Gut microbiome in health and disease: emerging diagnostic opportunities. *Gastroenterol Clin North Am* **48**, 221-235
6. Tang, W.H., Kitai, T., and Hazen, S.L. (2017) Gut microbiota in cardiovascular health and disease. *Circ Res* **120**, 1183-1196

7. Sára, M., and Sleytr, U.B. (2000) Bacterial S-layers. *J Bacteriol* **182**, 859-868
8. Zhu, C., Guo, G., Ma, Q., Zhang, F., Ma, F., Liu, J., Xiao, D., Yang, X., and Sun, M. (2017) Diversity in S-layers. *Prog Biophys Mol Biol* **123**, 1-15
9. Fagan, R.P., and Fairweather, N.F. (2014) Biogenesis and functions of bacterial S-layers. *Nat Rev Microbiol* **12**, 211-222
10. Gerbino, E., Carasi, P., Mobili, P., Serradell, M.A., and Gómez-Zavaglia, A. (2015) Role of S-layer proteins in bacteria. *World J Microbiol Biotechnol* **31**, 1877-1887
11. Malamud, M., Bolla, P.A., Carasi, P., Gerbino, E., Gómez-Zavaglia, A., Mobili, P., and Serradell, M.A. (2019) S-layer proteins from lactobacilli: biogenesis, structure, functionality and biotechnological applications, in *Lactobacillus Genomics and Metabolic Engineering*, Caister Academic Press, Poole, UK, pp 105-130
12. Pum, D., and Sleytr, U.B. (2014) Reassembly of S-layer proteins. *Nanotechnology* **25**, 312001
13. Garrote, G.L., Delfederico, L., Bibiloni, R., Abraham, A.G., Pérez, P.F., Semorile, L., and De Antoni, G.L. (2004) Lactobacilli isolated from kefir grains: evidence of S-layer proteins. *J Dairy Res* **71**, 222-230
14. Malamud, M., Carasi, P., Bronsoms, S., Trejo, S.A., and Serradell, M.A. (2017) *Lactobacillus kefiri* shows inter-strain variations in the amino acid sequence of the S-layer proteins. *Antonie Van Leeuwenhoek* **110**, 515-530
15. Cavallero, G., Malamud, M., Casabuono, A.G., Serradell, M.A., and Couto, A.S. (2017) A glycoproteomic approach reveals that the S-layer glycoprotein from *Lactobacillus kefiri* CIDCA 83111 is O- and N-glycosylated. *J Proteomics* **162**, 20-29
16. Rodrigues-Oliveira, T., Belmok, A., Vasconcellos, D., Schuster, B., and Kyaw, C.M. (2017) Archaeal S-layers: overview and current state of the art. *Front Microbiol* **8**, 2597
17. Chinthamani, S., Settem, R.P., Honma, K., Kay, J.G., and Sharma, A. (2017) Macrophage inducible C-type lectin (Mincle) recognizes glycosylated surface (S)-layer of the periodontal pathogen *Tannerella forsythia*. *PLoS One* **12**, e0173394
18. Richards, E., Bouché, L., Panico, M., Arbeloa, A., Vinogradov, E., Morris, H., Wren, B., Logan, S.M., Dell, A., and Fairweather, N.F. (2018) The S-layer protein of a *Clostridium difficile* SLCT-11 strain displays a complex glycan required for normal cell growth and morphology. *J Biol Chem* **293**, 18123–18137
19. Konstantinov, S.R., Smidt, H., de Vos, W.M., Bruijns, S.C., Singh, S.K., Valence, F., Molle, D., Lortal, S., Altermann, E., Klaenhammer, T.R., and van Kooyk, Y. (2008) S layer protein A of *Lactobacillus acidophilus* NCFM regulates immature dendritic cell and T cell functions.*Proc Natl Acad Sci USA* **105**, 19474–19479
20. Liu, Z., Ma, Y., Shen, T., Chen, H., Zhou, Y., Zhang, P., Zhang, M., Chu, Z., and Qin, H. (2011) Identification of DC-SIGN as the receptor during the interaction of *Lactobacillus plantarum* CGMCC 1258 and dendritic cells. *World J Microbiol Biotechnol* **27**, 603-611
21. Prado Acosta, M., Palomino, M. M., Allievi, M.C., Sánchez Rivas, C., and Ruzal, S.M. (2008) Murein hydrolase activity in the surface layer of *Lactobacillus acidophilus* ATCC 4356. *Appl Environ Microbiol* **74**, 7824–7827
22. Malamud, M., Carasi, P., Freire, T., and Serradell, M.L.A. (2018) S-layer glycoprotein from Lactobacillus kefiri CIDCA 8348 enhances macrophages response to LPS in a Ca+2-dependent manner. *Biochem Biophys Res Commun* **495**, 1227–1232
23. Malamud, M., Carasi, P., Assandri, M.H., Freire, T., Lepenies, B., and Serradell, M.A. (2019) S-layer glycoprotein from *Lactobacillis kefiri* exerts its immunostimulatory activity through glycan recognition by Mincle. *Front Immunol* **10**, 1422
24. Mobili P, Serradell MA, Trejo SA, Aviles Puigvert FX, Abraham AG, De Antoni GL. (2009) Heterogeneity of S-layer proteins from aggregating and non-aggregaing *Lactobacillus kefiri* strains. *Antonie Van Leeuwenhoek* **95,** 363–372

25. Carasi P, Ambrosis NM, De Antoni GL, Bressollier P, Urdaci MC, Serradell MA (2014). Adhesion properties of potentially probiotic *Lactobacillus kefiri* to gastrointestinal mucus. *J Dairy Res* **81**, 16–23
26. Palmisano, G., Melo-Braga, M.N., Engholm-Keller, K., Parker, B.L., and Larsen, M.R. (2012) Chemical deamidation: a common pitfall in large-scale N-linked glycoproteomic mass spectrometry-based analyses. *J Proteome Res* **11**, 1949-1957
27. del Fresno, C., Iborra, S., Saz-Leal, P., Martínez-López, M., and Sancho, D. (2018) Flexible signaling of myeloid C-type lectin receptors in immunity and inflammation. *Front Immunol* **9**, 804.
28. Möschl, A., Schäffer, C., Sleytr, U. B., Messner, P., Christian, R., and Schulz, G. (1993) Characterization of the S-layer glycoproteins of two lactobacilli, in *Advances in bacterial paracrystalline surface layer*, Springer, Boston, MA, pp. 281-284
29. Anzengruber, J., Pabst, M., Neumann, L., Sekot, G., Heinl, S., Grabherr, R., Altmann, F., Messner, P., and Schäffer, C. (2014) Protein O-glucosylation in *Lactobacillus buchneri*. *Glycoconj J* **31**, 117–131
30. Fina Martín, J., Palomino, M.M., Cutine, A.M., Modenutti, C.P., Fernández Do Porto, D.A., Allievi, M.C., Zanini, S.H., Mariño, K.V., Barquero, A.A., and Ruzal, S.M. (2019) Exploring lectin-like activity of the S-layer protein of *Lactobacillus acidophilus* ATCC 4356. *Appl Microbiol Biotechnol* **103**, 4839-4857
31. Messner, P., Steiner, K., Zarschler, K., and Schäffer, C. (2008) S-layer nanoglycobiology of bacteria. *Carbohydr Res* **343**, 1934–1951
32. Qazi, O., Hitchen, P., Tissot, B., Panico, M., Morris, H.R., Dell, A., and Fairweather, N. (2009) Mass spectrometric analysis of the S-layer proteins from *Clostridium difficile* demonstrates the absence of glycosylation. *J Mass Spectrom* **44**, 368-374
33. Lightfoot, Y.L., Selle, K., Yang, T., Goh, Y.J., Sahay, B., Zadeh, M., Owen, J.L., Colliou, N., Li, E., Johannssen, T., Lepenies, B., Klaenhammer, T.R., and Mohamadzadeh, M. (2015) SIGNR3-depndent immune regulation by *Lactobacillus acidophilus* surface layer protein A in colitis. *EMBO J* **34**, 881-895
34. Devi, S., Rajakumara, E., and Ahmed, N. (2015) Induction of Mincle by *Helicobacter pylori* and consequent anti-inflammatory signalling denote a bacterial survival strategy. *Sci Rep* **5,** 15049
35. Garrote, G.L., Abraham, A.G., and De Antoni, G.L. (2001) Chemical and microbiological characterisation of kefir grains. *J Dairy Res* **68**, 639-652
36. Carasi, P., Trejo, F.M., Pérez, P.F., De Antoni, G.L. and Serradell, M.A. (2012) Surface proteins of *Lactobacillus kefir* antagonize *in vitro* cytotoxic effect of *Clostridium difficile* toxins. *Anaerobe* **18**, 135-142
37. Morelle, W., and Michalski, J.C. (2007) Analysis of protein glycosylation by mass spectrometry. *Nat Protoc* **2**, 1585-1602
38. Selman, M.H., Hemayatkar, M., Deelder, A.M., and Wuhrer, M. (2011) Cotton HILIC SPE microtips for microscale purification and enrichment of glycans and glycopeptides. *Anal Chem* **83**, 2492-2499
39. Mayer, S., Moeller, R., Monteiro, J.T., Ellrott, K., Josenhans, C., and Lepenies, B. (2018) C-type lectin receptor (CLR)-Fc fusion proteins as tools to screen for novel CLR/bacteria interactions: an exemplary study on preselected *Campylobacter jejuni* isolates. *Front Immunol* **9**, 213
40. Kostarnoy, A.V., Gancheva, P.G., Lepenies, B., Tukhvatulin, A.I., Dzharullaeva, A.S., Polyakov, N.B., Grumov, D.A., Egorova, D.A., Kulibin, A.Y., Bobrov, M.A., Malolina, E.A., Zykin, P.A., Soloviev, A.I., Riabenko, E., Maltseva, D.V., Sakharov, D.A., Tonevitsky, A.G., Verkhovskaya, L.V., Logunov, D.Y., Naroditsky, B.S. and Gintsburg A.L. (2017) Receptor Mincle promotes skin allergies and is capable of recognizing cholesterol sulfate. *Proc Natl Acad Sci U S A* **114,** E2758-E2765
41. Eriksson, M., Johannssen, T., von Smolinski, D., Gruber, A.D., Seeberger, P.H. and Lepenies B. (2013) The C-type lectin receptor SIGNR3 binds to fungi present in commensal Microbiota and influences immune regulation in experimental colitis. *Front Immunol* **4**, 196

42. Heß, R., Storcksdieck Genannt Bonsmann, M., Lapuente, D., Maaske, A., Kirschning, C., Ruland, J., Lepenies, B., Hannaman, D., Tenbusch, M. and Überla, K. (2019) Glycosylation of HIV Env impacts IgG subtype responses to vaccination. *Viruses* **11**, pii: E153
43. Monteiro, J.T., Schön, K., Ebbecke, T., Goethe, R., Ruland, J., Baumgärtner, W., Becker, S.C., and Lepenies, B. (2019) The CARD9-associated C-type lectin, Mincle, recognizes La Crosse virus (LACV) but plays a limited role in early antiviral responses against LACV. *Viruses* **11,** pii: E303
44. Perez-Riverol Y., Csordas A., Bai, J., Bernal-Llinares, M., Hewapathirana, S., Kundu, D.J., Inuganti, A., Griss, J., Mayer, G., Eisenacher, M., Pérez, E., Uszkoreit, J., Pfeuffer, J., Sachsenberg, T., Yilmaz, S., Tiwary, S., Cox, J., Audain, E., Walzer, M., Jarnuczak, A.F., Ternent, T., Brazma, A., Vizcaíno, J.A. (2019) The PRIDE database and related tools and resources in 2019: improving support for quantification data. *Nucleic Acids Res* **47(D1):** D442-D450 (PubMed ID: 30395289)

Figure Legends:

Figure 1. Analysis by HPAEC-PAD of the sugar components of the *O*-glycosidic chains released by reductive β-elimination. *A, B* and *C,* neutral monosaccharides released from SLP-5818, SLP-8348 and SLP-8321 respectively. *D, E* and *F*, alditols released from SLP-5818, SLP-8348 and SLP-8321 respectively. Glc: Glucose; Gal: Galactose; Man: Mannose; $GalNH_2$: Galactosamine; $GlcNH_2$: Glucosamine.

Figure 2. ***O*-glycopeptide analysis by nanoHPLC-ESI-Orbitrap of SLP-5818.** *A*, Selected MS2 spectra, *m/z* 1537.8352. (y and b peptide fragments and Y glycan-peptide fragments are indicated). *B*, Full MS spectrum at retention time 19.89 min showing signals corresponding to 147-170 unmodified peptide and to the same peptide bearing one or two hexose units.

Figure 3. *O*-glycopeptide analysis. *A, B*, Full MS spectra of SLP-8348 and SLP-8321 respectively, showing glycopeptide families with charge +4, +5, +6 and +7. *C*, MS/MS spectra of ion *m/z* 1119, 8097^{+6} from SLP-8348. *D*, MS/MS spectra of ion *m/z* 1597.6873^{+4} from SLP-8321 (y and b peptide fragments and hexose fragments are indicated).

Figure 4. *N*-Glycosylation analysis of SLP-5818. *A*, WGA-Sepharose analysis: lane 1: Lectin bound glycoprotein, lane 2: SLP extract, lane 3: MW markers. MS2 spectra of enzymatically deglycosylated peptides: *B*, peptide 51-63 and *C*, peptide 450-461, containing the 0.9846 Da mass increase derived from Asn/Asp conversion. Differences between the *in silico* digested peptides (b and y ions in the inset) and the experimental masses are highlighted in blue.

Figure 5. *A*, NanoHPLC-ESI-Orbitrap analysis of permethylated *N*-glycans. a) Total ion current chromatogram. Extracted ion chromatograms of permethylated oxonium ions: b) *m/z* 464.24 (Hex-HexNAc oxonium ion); c) *m/z* 189.11 (dHex oxonium ion). ▲ dHex; ● , ● Hex; ■ HexNAc. *B*, MALDI-TOF MS spectrum of permethylated *N*-glycans.

Figure 6. Selected MS2 spectra of permethylated *N*-glycans detected by nanoHPLC-ESI-Orbitrap analysis. *A, m/z* 1009.5226. *B, m/z* 886.9614. ▲ dHex; ● , ● Hex; ■ HexNAc.

Figure 7. Modulation of LPS-induced maturation of macrophages by *L. kefiri* SLP-8321 and SLP-5818. *A*, IL-6 concentration (pg/mL) by capture ELISA in the supernatant of the murine RAW 264.7 cultures after 24 h of stimulation. *B*, Percentage of CD40+ and CD86+ RAW 264.7 cells after 24 h of stimulation. A representative figure of three independent experiments is shown (±SD, indicated by error bars). *P< 0.05; n.s: not significant.

Figure 8. C-type Lectin Receptor recognition of SLP-8321 and SLP-5818. *A*, Reactivity of CLR-hFc fusion proteins on SLP was evaluated by an ELISA type assay (using the same experimental model as in Ref. 23). *B*, Inhibition assays were performed using EGTA, a Ca^{2+} chelating agent. These are representative figures of three independent experiments (±SD, indicated by error bars).

Figure 9. SLP-8321 and SLP-5818 are recognized by specific CLRs expressed on BMDCs. *A*, Binding (4°C, squares) and internalization (37°C, circles) of Atto 647N-labeled-SLP at different concentrations on CD11c+ cells from C57BL/6 and CLR-deficient mice. *B*, Level of IL-6 and TNF-α in culture supernatant of BMDCs from C57BL/6 and CLR-deficient mice after stimulation with SLPs, LPS or the combination of both for 24h. *C*, Cell surface expression of CD40 and CD86 on CD11c+ cells from C57BL/6 and CLR-deficient mice after stimulation with SLPs, LPS or the combination of both for 24h. A representative figure of three independent experiments is shown, following the same experimental lines described in Ref. 23 (±SD, indicated by error bars). *P<0.05; n.s: not significant; KO: knock-out.

Figure 10. CLR-SLP specific interactions impact on T-cell stimulatory function of the SLP-activated BMDCs. Cells from C57BL/6 and CLR-deficient mice were stimulated with SLP, OVA or the combination of both for 24h and then exposed to CFSE-labelled CD4+ T cells from OT-II mice using the same experimental model as in Ref. 23. *A*, IFN-γ level in supernatants measured after five days. *B*, Proliferation index of CD4+ T cells. A representative figure of three independent experiments is shown (±SD, indicated by error bars). *P<0.05; n.s: not significant; KO: knock-out.

.

Table 1: O-linked glycosylated peptides of *L. kefiri* CIDCA 5818 S-layer protein

Peptide	Glycoform	m/z M^{+3} (calc.)	m/z M^{+3} (exp.)	error (ppm)
^{147}2256.0353^{170}	Hex_1	807.0367	807.0370	-0.41
	Hex_2	861.0543	861.0551	-0.97
	Hex_3	915.0719	915.0724	-0.58
	Hex_4	969.0895	969.0895	-0.03
	Hex_5	1023.1071	1023.1075	-0.42
	Hex_6	1077.1247	1077.1252	-0.50
	Hex_7	1131.1423	1131.1429	-0.56
	Hex_8	1185.1599	1185.1581	1.49
	Hex_9	1239.1775	1239.1770	0.38
	Hex_{10}	1293.1951	1293.1959	-0.64
	Hex_{11}	1347.2127	1347.2139	-0.92
	Hex_{12}	1401.2303	1401.2311	-0.59
	Hex_{13}	1455.2479	1455.2474	0.32
	Hex_{14}	1509.2655	1509.2646	0.57
	Hex_{15}	1563.2831	1563.2825	0.36
	Hex_{16}	1617.3007	1617.3018	-0.70
	Hex_{17}	1671.3183	1671.3114	4.11
	Hex_{18}	1725.3359	1725.3359	-0.02
	Hex_{19}	1779.3535	1779.3544	-0.52
	Hex_{20}	1833.3711	1833.3687	1.29
	Hex_{21}	1887.3887	1887.3909	-1.18
	Hex_{22}	1941.4063	1941.4103	-2.08
	Hex_{23}	1995.4239	1995.4330	-4.58

Table 2: O-linked glycosylated peptides of *L. kefiri* CIDCA 8348 S-layer protein

Peptide	Glycoform	m/z M^{+4} (calc.)	m/z M^{+4} (exp.)	error (ppm)
^{125}4277.0207^{170}	hex_{22}	1961.5529	1961.5544	-0.78
	hex_{21}	1921.0397	1921.0396	0.04
	hex_{20}	1880.5265	1880.5272	-0.39
	hex_{19}	1840.0133	1840.0141	-0.45
	hex_{18}	1799.5001	1799.5057	-3.13
	hex_{17}	1758.9869	1758.9868	0.04
	hex_{16}	1718.4737	1718.4769	-1.88
	hex_{15}	1677.9605	1677.9602	0.16
	hex_{14}	1637.4473	1637.4468	0.29
	hex_{13}	1596.9341	1596.9348	-0.45
	hex_{12}	1556.4209	1556.4201	0.50
	hex_{11}	1515.9077	1515.9086	-0.61
	hex_{10}	1475.3945	1475.3951	-0.42
	hex_{9}	1434.8813	1434.8822	-0.64
	hex_{8}	1394.3681	1394.3696	-1.09
	hex_{7}	1353.8549	1353.8557	-0.61
	hex_{6}	1313.3417	1313.3422	-0.40

Table 3: O-linked glycosylated peptides of *L. kefiri* CIDCA 8321 S-layer protein

Peptide	Glycoform	m/z M^{+4} (calc.)	m/z M^{+4} (exp.)	Error (ppm)
^{125}4277.0207^{170}	hex_{22}	1961.5529	1961.5525	0.19
	hex_{21}	1921.0397	1921.0369	1.44
	hex_{20}	1880.5265	1880.5252	0.68
	hex_{19}	1840.0133	1840.0122	0.58
	hex_{18}	1799.5001	1799.5038	-2.07
	hex_{17}	1758.9869	1758.9854	0.84
	hex_{16}	1718.4737	1718.4721	0.92
	hex_{15}	1677.9605	1677.9615	-0.61
	hex_{14}	1637.4473	1637.4498	-1.54
	hex_{13}	1596.9341	1596.9349	-0.52
	hex_{12}	1556.4209	1556.4187	1.40
	hex_{11}	1515.9077	1515.9091	-0.94
	hex_{10}	1475.3945	1475.3958	-0.90
	hex_{9}	1434.8813	1434.8829	-1.13
	hex_{8}	1394.3681	1394.3687	-0.45
	hex_{7}	1353.8549	1353.8516	2.42
	hex_{6}	1313.3417	1313.3427	-0.78
	Hex_{5}	1272.8285	1272.8290	-0.41
	Hex_{4}	1232.3153	1232.3162	-0.75

Table 4: Summary of main N-glycan structures determined in *L. kefiri* JCM 5818 surface layer protein.

N-glycan	$[M+H]^{++}$ *m/z* (calc.)	$[M+H]^{++}$ *m/z* (Obs.)	Error (ppm)
HexNAc4-Hex5-dHex	1111.5749	1111.5746	0.3
HexNAc4-Hex4-dHex	1009.525	1009.5243	0.7
HexNAc3-Hex4-dHex	886.96185	886.962	0.2
HexNAc4-Hex3-dHex	907.4751	907.4769	2.0
HexNAc4-Hex5	1024.5303	1024.5303	0.0
HexNAc4-Hex4	922.4804	922.4775	3.1

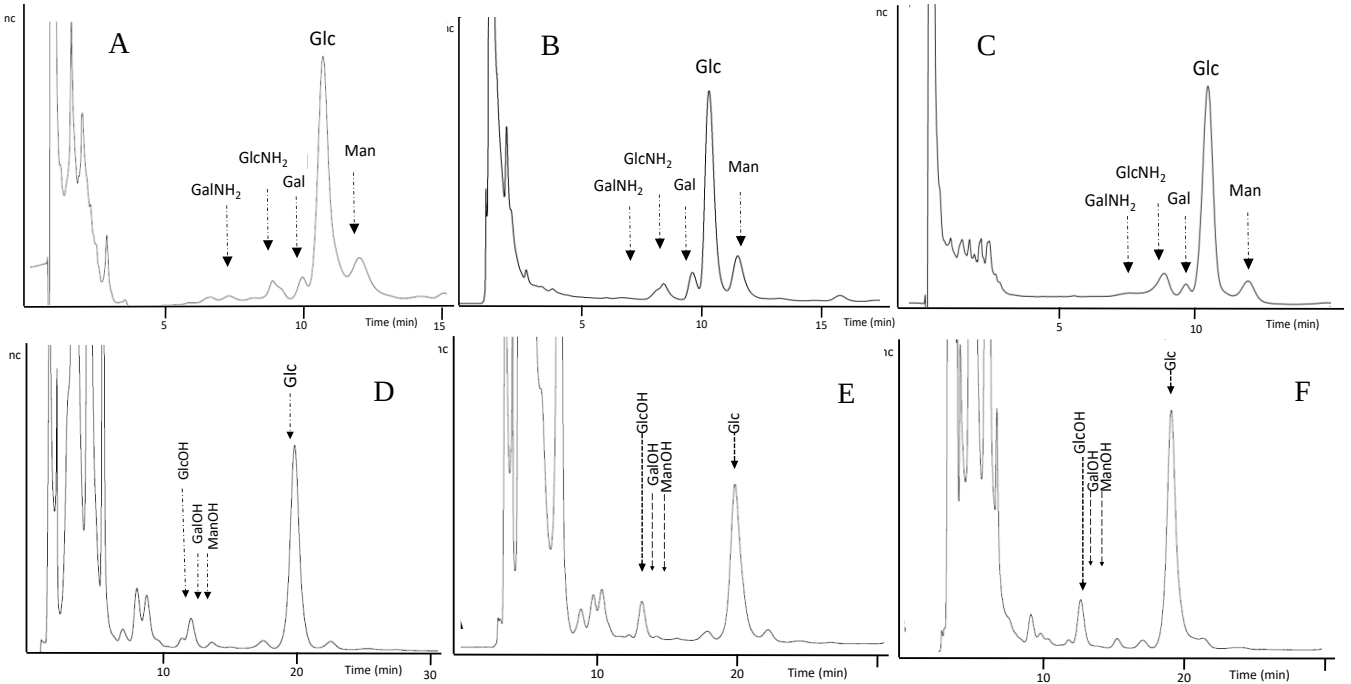
A
Glc
GlcNH2
GalNH2
Gal
Man
Time (min)
B
Glc
GlcNH2
GalNH2
Gal
Man
Time (min)
C
Glc
GlcNH2
GalNH2
Gal
Man
Time (min)
D
Glc
GlcOH
GalOH
ManOH
Time (min)
E
GlcOH
GalOH
ManOH
Glc
Time (min)
F
Glc
GlcOH
GalOH
ManOH
Time (min)

Figure 1.

A

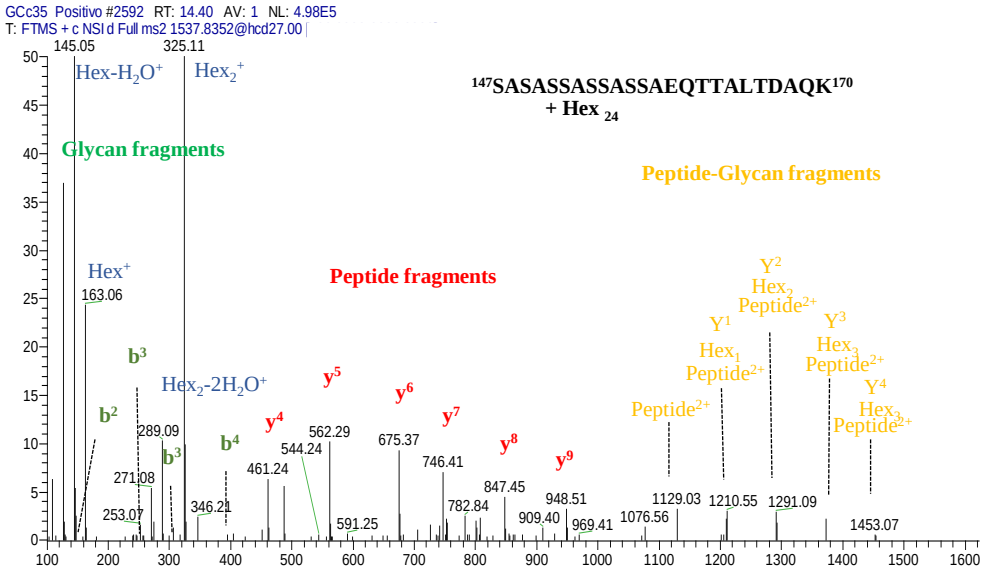
GCc35 Positivo #2592 RT: 14.40 AV: 1 NL: 4.98E5
T: FTMS + c NSI d Full ms2 1537.8352@hcd27.00
147SASASSASSASSAEQTTALTDAQK170
+ Hex 24
Glycan fragments
Peptide fragments
Peptide-Glycan fragments
Hex-H2O+
Hex2+
Hex+
Hex2-2H2O+
b2
b3
b4
y4
y5
y6
y7
y8
y9
Y1
Y2
Y3
Y4
Hex1 Peptide2+
Hex2 Peptide2+
Hex3 Peptide2+
Peptide2+
145.05
163.06
253.07
271.08
289.09
325.11
346.21
461.24
544.24
562.29
591.25
675.37
746.41
782.84
847.45
909.40
948.51
969.41
1076.56
1129.03
1210.55
1291.09
1453.07

B

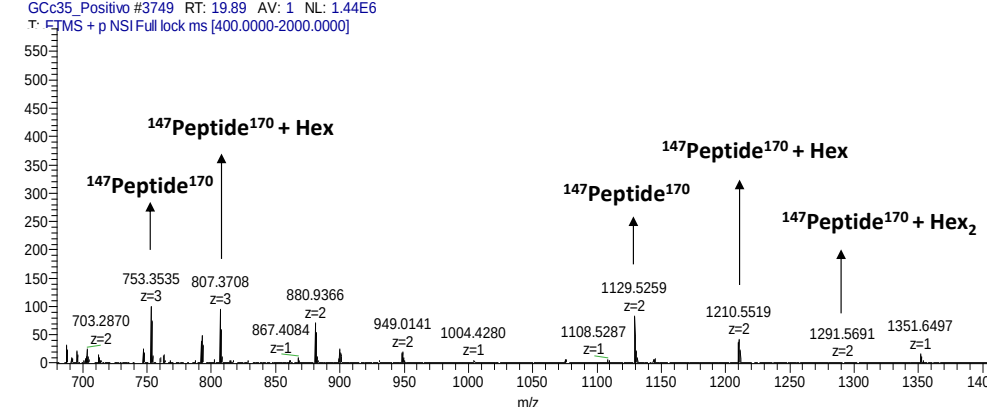
GCc35_Positivo #3749 RT: 19.89 AV: 1 NL: 1.44E6
T: FTMS + p NSI Full lock ms [400.0000-2000.0000]
147Peptide170 + Hex
147Peptide170
147Peptide170 + Hex
147Peptide170
147Peptide170 + Hex2
703.2870 z=2
753.3535 z=3
807.3708 z=3
867.4084 z=1
880.9366 z=2
949.0141 z=2
1004.4280 z=1
1108.5287 z=1
1129.5259 z=2
1210.5519 z=2
1291.5691 z=2
1351.6497 z=1
m/z

Figure 2

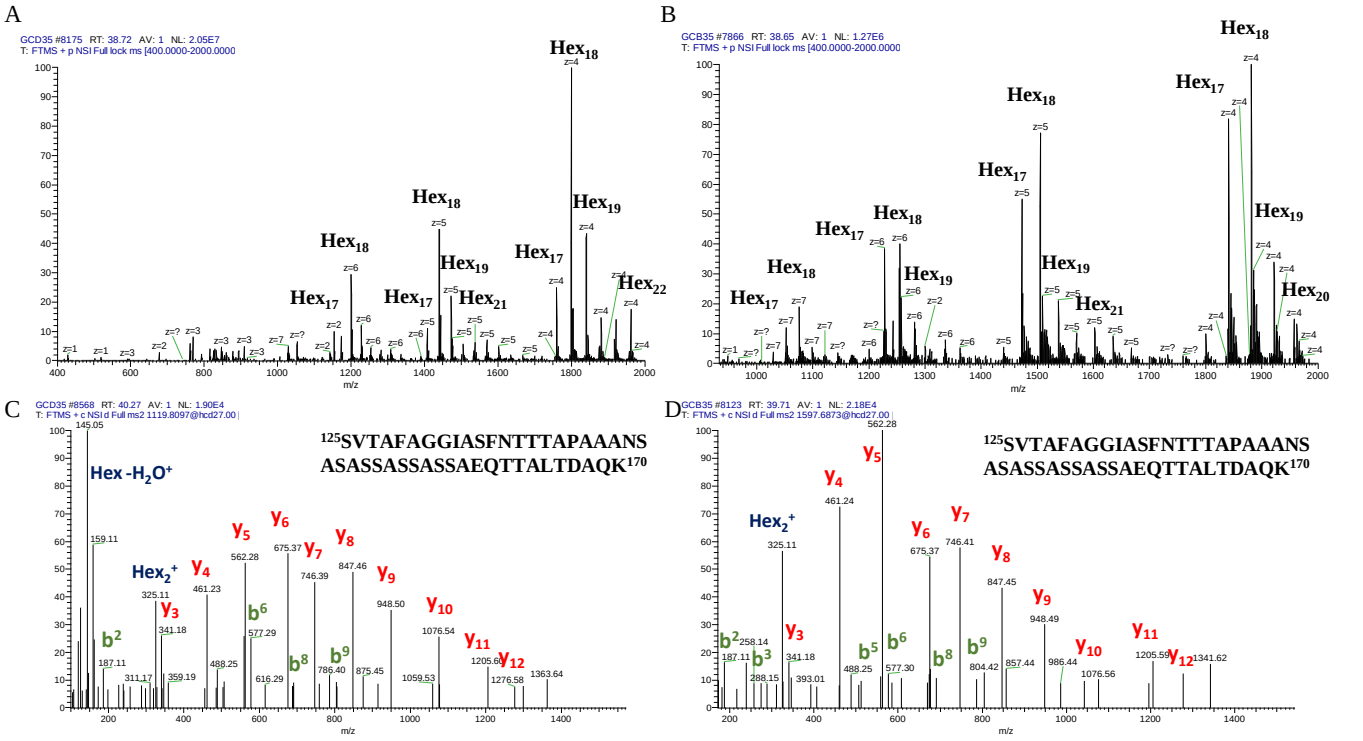
A
GCD35 #8175 RT: 38.72 AV: 1 NL: 2.05E7
T: FTMS + p NSI Full lock ms [400.0000-2000.0000
Hex18
Hex19
Hex18
Hex18
Hex17
Hex17
Hex19
Hex21
Hex17
Hex22
m/z
B
GCB35 #7866 RT: 38.65 AV: 1 NL: 1.27E6
T: FTMS + p NSI Full lock ms [400.0000-2000.0000
Hex18
Hex17
Hex18
Hex17
Hex18
Hex17
Hex19
Hex18
Hex19
Hex21
Hex19
Hex20
m/z
C
GCD35 #8568 RT: 40.27 AV: 1 NL: 1.90E4
T: FTMS + c NSI d Full ms2 1119.8097@hcd27.00
125SVTAFAGGIASFNTTTAPAAANS
ASASSASSASSAEQTTALTDAQK170
Hex -H2O+
Hex2+
m/z
D
GCB35 #8123 RT: 39.71 AV: 1 NL: 2.18E4
T: FTMS + c NSI d Full ms2 1597.6873@hcd27.00
125SVTAFAGGIASFNTTTAPAAANS
ASASSASSASSAEQTTALTDAQK170
Hex2+
m/z

Figure 3.

A

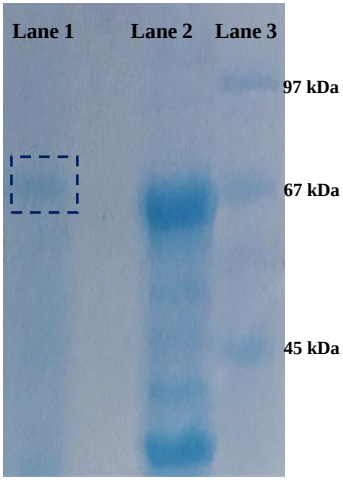

B

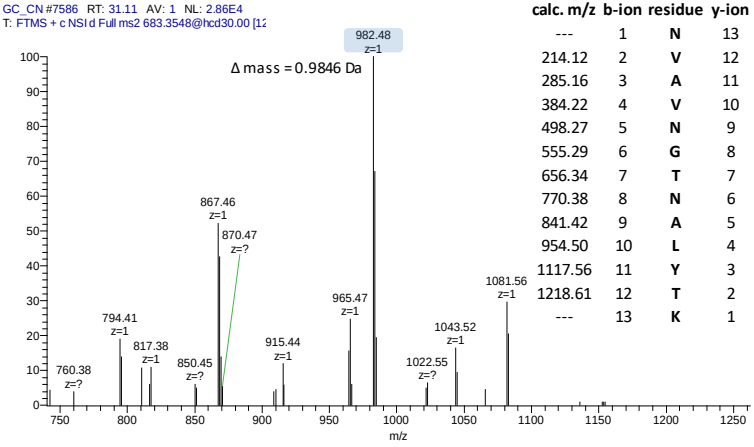

calc. m/z	b-ion	residue	y-ion	calc. m/z
---	1	N	13	---
214.12	2	V	12	1250.67
285.16	3	A	11	1151.61
384.22	4	V	10	1080.57
498.27	5	N	9	981.50
555.29	6	G	8	867.46
656.34	7	T	7	810.44
770.38	8	N	6	709.39
841.42	9	A	5	595.35
954.50	10	L	4	524.31
1117.56	11	Y	3	411.22
1218.61	12	T	2	248.16
---	13	K	1	147.11

C

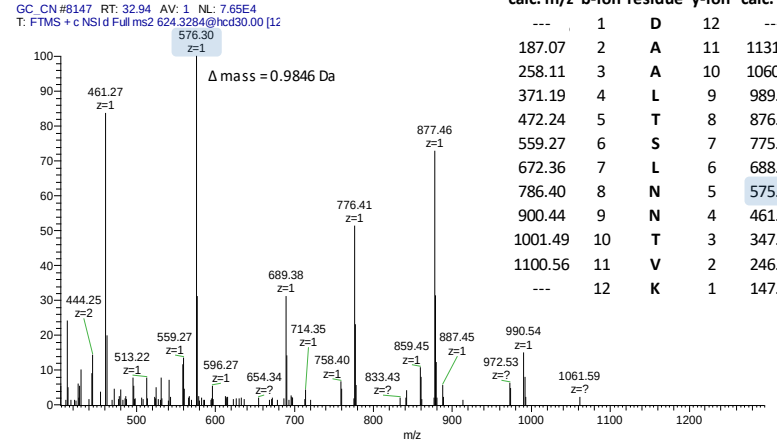

calc. m/z	b-ion	residue	y-ion	calc. m/z
---	1	D	12	---
187.07	2	A	11	1131.64
258.11	3	A	10	1060.60
371.19	4	L	9	989.56
472.24	5	T	8	876.48
559.27	6	S	7	775.43
672.36	7	L	6	688.40
786.40	8	N	5	575.31
900.44	9	N	4	461.27
1001.49	10	T	3	347.23
1100.56	11	V	2	246.18
---	12	K	1	147.11

Figure 4.

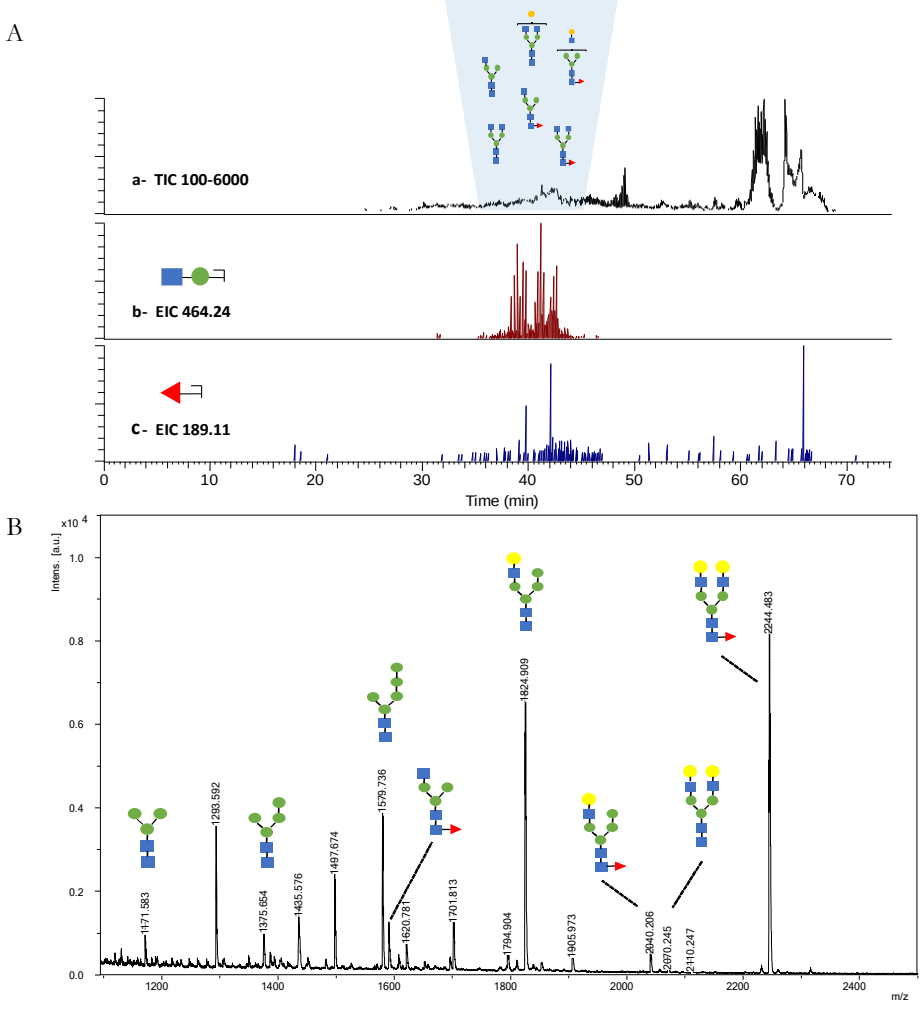
A
a- TIC 100-6000
b- EIC 464.24
C- EIC 189.11
0
10
20
30
40
50
60
70
Time (min)
B
x10 4
Intens. [a.u.]
1.0
0.8
0.6
0.4
0.2
0.0
1171.583
1293.592
1375.654
1435.576
1497.674
1579.736
1620.781
1701.813
1794.904
1824.909
1905.973
2040.206
2070.245
2110.247
2244.483
1200
1400
1600
1800
2000
2200
2400
m/z

Figure 5.

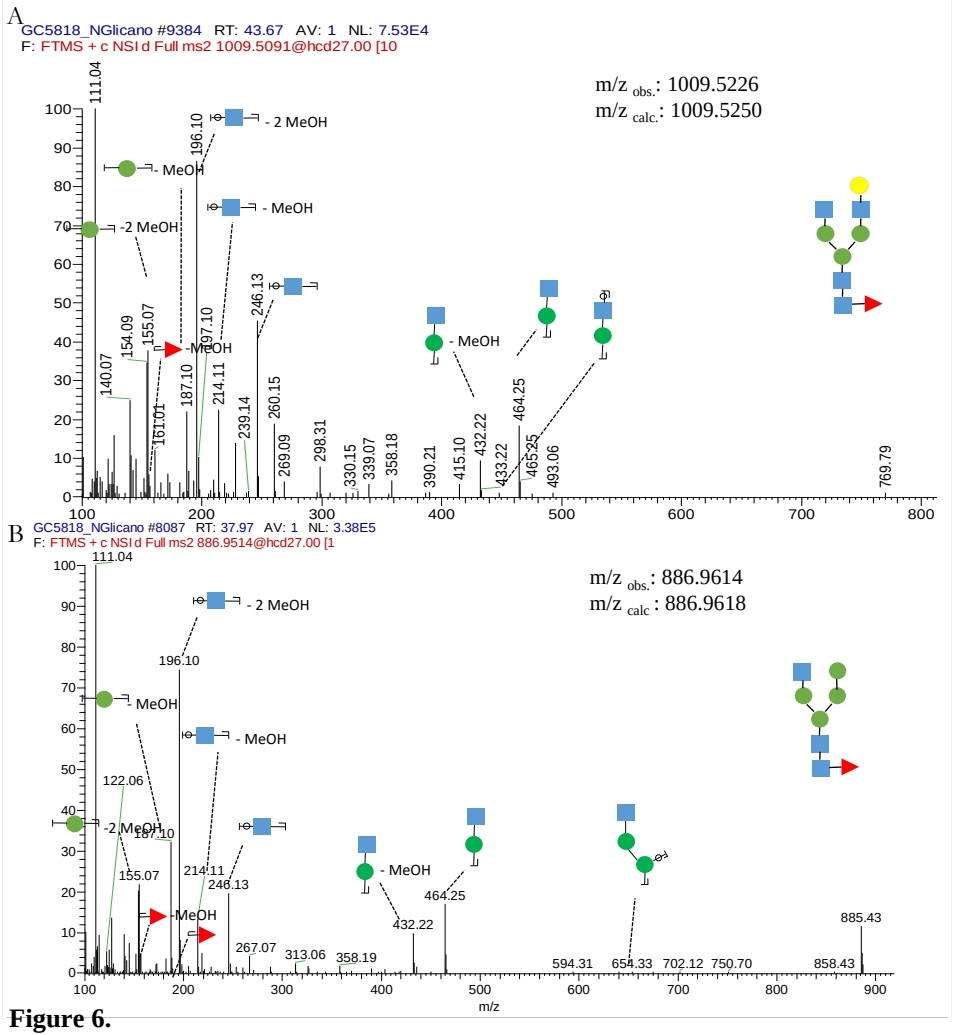
A
GC5818_NGlicano #9384 RT: 43.67 AV: 1 NL: 7.53E4
F: FTMS + c NSI d Full ms2 1009.5091@hcd27.00 [10
m/z obs.: 1009.5226
m/z calc.: 1009.5250
- 2 MeOH
- MeOH
- MeOH
-2 MeOH
- MeOH
-MeOH
111.04
196.10
246.13
155.07
154.09
197.10
140.07
187.10
214.11
239.14
260.15
161.01
298.31
269.09
330.15
339.07
358.18
390.21
415.10
432.22
433.22
464.25
465.25
493.06
769.79
B
GC5818_NGlicano #8087 RT: 37.97 AV: 1 NL: 3.38E5
F: FTMS + c NSI d Full ms2 886.9514@hcd27.00 [1
m/z obs.: 886.9614
m/z calc: 886.9618
- 2 MeOH
- MeOH
- MeOH
-2 MeOH
- MeOH
-MeOH
111.04
196.10
122.06
167.10
155.07
214.11
246.13
267.07
313.06
358.19
432.22
464.25
594.31
654.33
702.12
750.70
858.43
885.43
m/z

Figure 6.

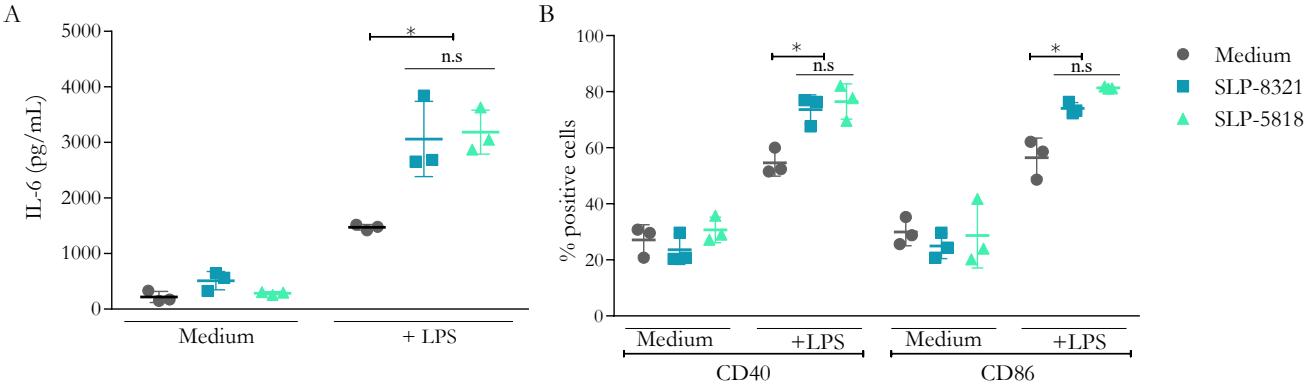
A
IL-6 (pg/mL)
5000
4000
3000
2000
1000
0
*
n.s
Medium
+ LPS
B
% positive cells
100
80
60
40
20
0
*
n.s
*
n.s
Medium
+LPS
Medium
+LPS
CD40
CD86
Medium
SLP-8321
SLP-5818

Figure 7.

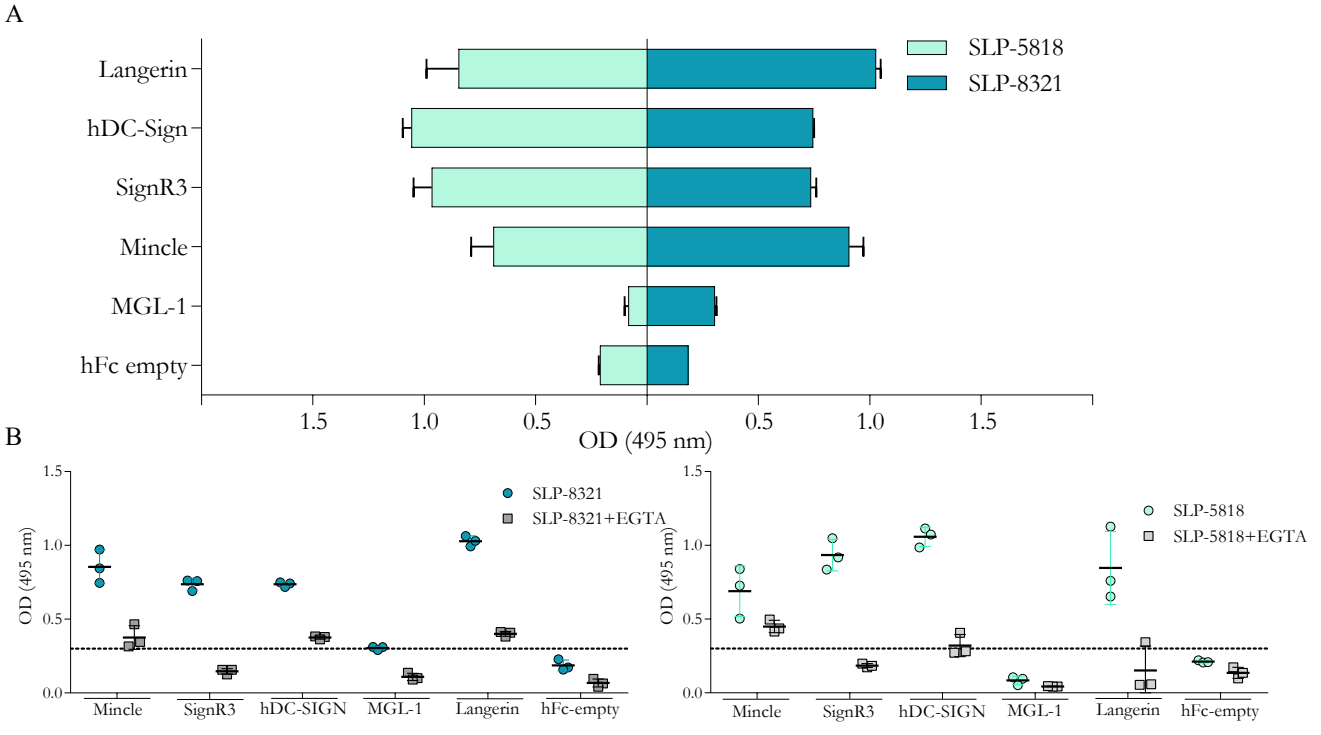
A
Langerin
hDC-Sign
SignR3
Mincle
MGL-1
hFc empty
SLP-5818
SLP-8321
1.5
1.0
0.5
0.5
1.0
1.5
OD (495 nm)
B
OD (495 nm)
SLP-8321
SLP-8321+EGTA
Mincle
SignR3
hDC-SIGN
MGL-1
Langerin
hFc-empty
SLP-5818
SLP-5818+EGTA

Figure 8.

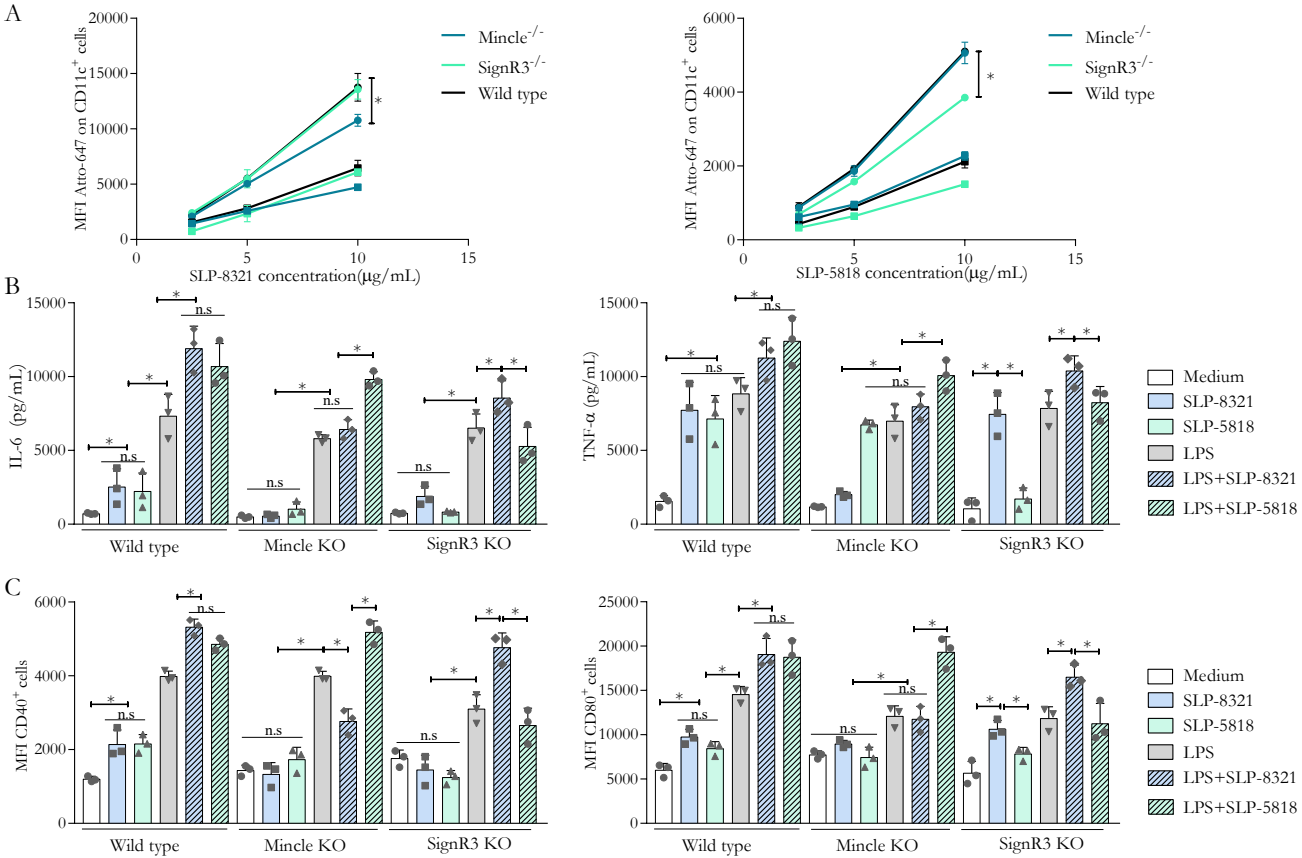
A
MFI Atto-647 on CD11c+ cells
SLP-8321 concentration(µg/mL)
Mincle-/-
SignR3-/-
Wild type
SLP-5818 concentration(µg/mL)
B
IL-6 (pg/mL)
TNF-α (pg/mL)
Wild type
Mincle KO
SignR3 KO
Medium
SLP-8321
SLP-5818
LPS
LPS+SLP-8321
LPS+SLP-5818
C
MFI CD40+ cells
MFI CD80+ cells
n.s

Figure 9.

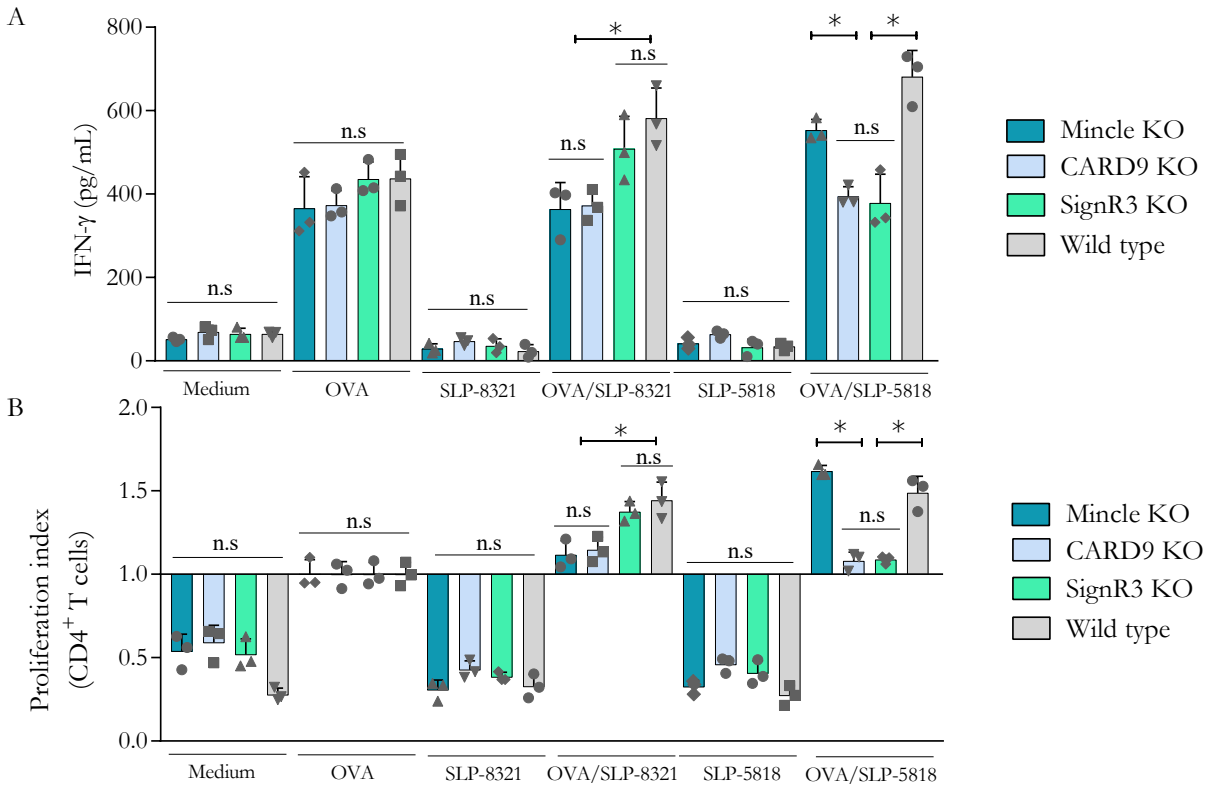
A
800
600
400
200
0
IFN-γ (pg/mL)
n.s
*
Medium
OVA
SLP-8321
OVA/SLP-8321
SLP-5818
OVA/SLP-5818
Mincle KO
CARD9 KO
SignR3 KO
Wild type
B
2.0
1.5
1.0
0.5
0.0
Proliferation index
(CD4+ T cells)

Figure 10.

Immunostimulation by *Lactobacillus kefiri* S-layer proteins with distinct glycosylation patterns requires different lectin partners

Mariano Malamud, Gustavo Cavallero, Adriana C Casabuono, Bernd Lepenies, María de los Angeles Serradell and Alicia S. Couto

J. Biol. Chem. published online August 13, 2020